 ISSN 2522-1841 (Online)
ISSN 0005-2531 (Print)

ANALYTICAL MODELING AND 3D VISUALIZATION OF THE T-X-Y PHASE DIAGRAM OF THE Bi_2S_3-Bi_2Se_3-BiI_3 SYSTEM

A.A.Qurbanov[1], E.J.Ahmadov[2*], A.I.Aghazade[2], G.F.Hasanov[2], F.S.Ibrahimova[2], I.J.Alverdiyev[1], A.N.Mammadov[2]

[1]*Ganja State University, Ganja, Azerbaijan*
[2]*"Institute of Chemistry" Public Legal Entity, MSE of the Azerbaijan Republic, Baku, Azerbaijan*
elvin.j.ahmadov@gmail.com

Received 03.02.2026
Reviewed 04.03.2026
Accepted 01.04.2026

Phase diagrams of boundary quasi-binary systems within the composition triangle of the Bi_2S_3–Bi_2Se_3–BiI_3 system (A) were investigated for selected compositions based on a limited number of DTA data and the solid-phase equilibrium diagram of system (A). Analytical equations were derived for the liquidus curves of phases in the boundary systems, as well as for the liquidus surfaces of solid solutions based on Bi_2S_3, Bi_2Se_3 compounds in system (A), and for the intermediate phases $BiS_{1-x}Se_xI$ and $Bi_{19}S_{27(1-x)}Se_{27x}I_3$. Based on the obtained equations, a 3D visualization of the liquidus surface of system (A) was performed, and the types and coordinates of mono- and nonvariant equilibria present in the system were determined. Using the constructed 3D model of the liquidus surface, several isopleth sections of the T–x–y phase diagram were developed and validated by DTA results obtained from a limited number of samples. The presented results can be applied to the synthesis and crystal growth of $BiS_{1-x}Se_xI$ and $Bi_{19}S_{27(1-x)}Se_{27x}I_3$ solid solutions with tunable composition and properties.

Keywords: *bismuth thio- and selenoiodides, phase diagram, liquidus surface, 3D analytical modeling, solid solutions.*

https://doi.org/10.59849/0005-2531.2026.3.62

Introduction

Bismuth-based semiconductor chalcohalide compounds (especially BiSI and BiSeI) and their phases derived from them occupy an important place in modern materials science due to their functional properties, and their electronic structure and optical characteristics have been extensively studied [1-3]. Owing to their high photosensitivity and suitable band gap values, these materials are considered promising candidates for photodetector and photovoltaic applications [4,5]. The electronic and elastic properties observed in structurally similar $A^5B^6C^7$-type compounds, together with their low thermal conductivity and favorable charge transport characteristics, further enhance their importance as ferroelectric and thermoelectric materials [6-8].

Recently, in addition to these properties, the discovery of Rashba spin splitting in BiTeX (X = I, Cl, Br) - type compounds have significantly increased interest in these materials [9,10]. This effect arises from strong spin–orbit interaction and is associated with the breaking of inversion symmetry in their crystal structure. As a result, these materials are considered promising candidates for applications in various areas of modern technology, particularly in the development of spintronic devices, and quantum computing systems [11-13].

The purposeful search, synthesis, and design of new multicomponent functional materials are based on a deep study of phase equilibria and thermodynamic properties in the relevant systems [14-18]. Obtaining solid

solutions formed by purposeful substitution of elements in these materials and whose composition can be changed within a certain interval is one of the most effective approaches to optimizing the required properties [19-21]. The findings on phase equilibria in certain quasi-ternary and reciprocal systems composed of chalcogenides and halides of V^A subgroup elements have been reported in several studies [22–28].

The phase relationships in the Bi_2S_3–Bi_2Se_3–BiI_3 (A) system were studied in detail in our previous [29-32] works based on the analysis of the results obtained by powder X-ray diffraction (PXRD), differential thermal analysis (DTA), scanning electron microscopy (SEM), and electromotive force (EMF) methods of equilibrated alloys. This article presents the results of analytical 3D modeling of the liquidus surface of the (A) system based on DTA results of a limited number of samples. The types and coordinates of non- and monovariant equilibria present in the system are determined, and some polythermal sections of the T-x-y phase diagram are constructed.

Analytical modeling of the phase diagram, particularly the 3D visualization of crystallization surfaces, enables the determination of optimal conditions for obtaining solid phases from liquid alloys in the studied system. For this purpose, literature data on boundary systems, together with a limited number of experimental DTA results, were utilized. At the initial stage, analytical expressions describing the liquidus surfaces of the boundary systems were established. All analytical dependencies were obtained using the "analysis" module of the OriginLab software.

2. Experimental Part

2.1. Synthesis

High-purity elements (≥99.999%, Alfa Aesar) were employed to synthesize the binary Bi_2S_3, Bi_2Se_3, BiI_3, and the ternary compounds BiSeI, BiSI, and $Bi_{19}S_{27}I_3$. Stoichiometric quantities, measured with 10^{-4} g precision, were co-melted at temperatures 30-50 K above their respective melting points in evacuated (~10^{-2} Pa) and flame-sealed quartz ampoules.

Due to the high vapor pressures of iodine, sulfur, and selenium, a modified split-tube furnace approach was adopted: the cold zone was maintained just below the boiling point of the volatile component, while the hot zone exceeded the compound's melting point by 30–50 K [33-35]. Taking into account the peritectic melting behavior of BiSeI and BiSI, the synthesized compounds were then ground, pelletized, and annealed at 750 K for 300 hours to ensure full homogenization. The phase purity was verified by PXRD and DTA, and the results were in agreement with the literature data. [24,36-38].

Intermediate alloys within the BiI_3-Bi_2S_3-Bi_2Se_3 quasi-ternary system (each ~0.5 g) were synthesized from stoichiometric mixtures of previously prepared binary and ternary compounds. The melting process was conducted between 600 and 1100 K, with temperatures selected according to the melting behavior of the constituent phases. Post-synthesis, alloys in the Bi_2S_3-BiSI-BiSeI-Bi_2Se_3 subsystem were treated at 700 K, whereas those in the BiSI-BiSeI-BiI_3 subsystem were treated at 600 K for 600 h to provide equilibrium.

2.2. Methods

All prepared alloys were examined by DTA using a multichannel system built on the "TC-08 Thermocouple Data Logger" (±2 K), with measurements performed at a heating rate of 7–10 K/min. Samples were sealed in quartz ampoules (0.5 cm inner diameter, 2.5–3 cm length, free volume ≤ 0.5 cm²). Despite the volatility of BiI_3, any composition changes during thermal analysis are negligible.

3. Result and discussion

3. 1. 3D modeling of the liquidus surface of the BiI_3-Bi_2S_3-Bi_2Se_3 system

The modeling of the BiI_3-Bi_2S_3-Bi_2Se_3 phase diagram was carried out according to the method described in [39-43] using the 3D

Table 1. Phase diagrams and analytical dependencies for their liquidus line of the BiI_3-Bi_2S_3, BiI_3-Bi_2Se_3 and Bi_2S_3-Bi_2Se_3 systems (equations are presented in computer variation)

Phase diagram	System, region	Equations: T,K=f(x)	Eq.N.
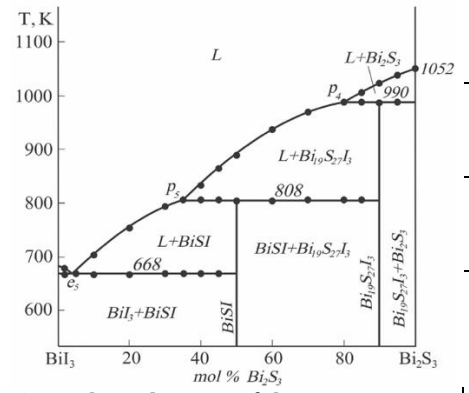 **Fig.1.** Phase diagram of the system BiI_3-Bi_2S_3 [37]	BiI_3-Bi_2S_3, liquidus BiI_3, x=*x*(BiJ_3)=0.97÷1	248+433*x	1
	BiI_3-Bi_2S_3, liquidus BiSI, x=*x*(BiJ_3)=0.65÷0.955	574+920*x-860*x^2	2
	BiI_3-Bi_2S_3, liquidus $Bi_{19}S_{27}I_3$, x=*x*(BiJ_3)=0.2÷0.65	993+106*x-600*x^2	3
	BiI_3-Bi_2S_3, Liquidus Bi_2S_3, x=*x*(BiI_3)=0÷0.2	1052-110*x-1000*x^2	4
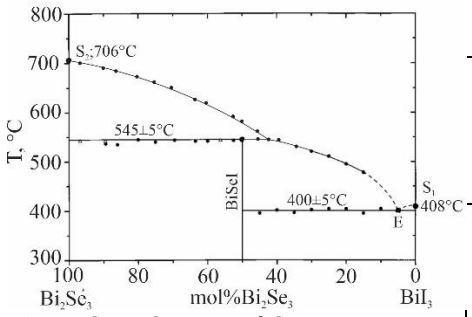 **Fig.2.** Phase diagram of the system BiI_3-Bi_2Se_3 [44, refined in this work]	BiI_3-Bi_2Se_3, liquidus Bi_2Se_3, x=*x*(BiI_3)= 0÷0.584	979-173*x-182*x^2	5
	BiI_3-Bi_2Se_3, liquidus BiSeI, x=*x*(BiI_3)= 0.584÷0.955	1830-4334*x+ 6317*x^2-3192*x^3	6
	BiI_3-Bi_2Se_3, liquidus BiI_3, x=*x*(BiJ_3)=0.955÷1	503+178*x	7
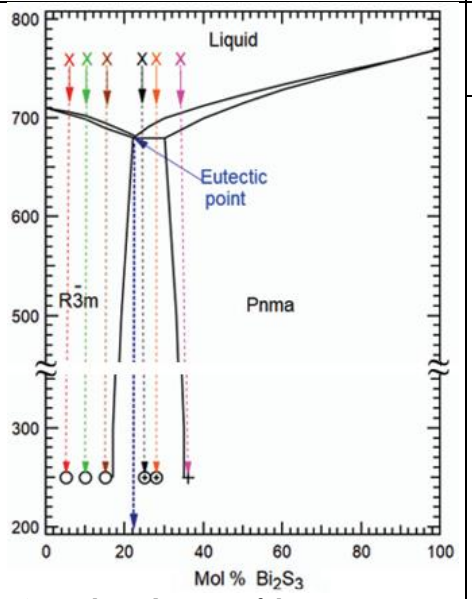 **Fig.3.** Phase diagram of the system Bi_2Se_3- Bi_2S_3 [45]	Bi_2S_3- Bi_2Se_3, liquidus Bi_2S_3, x=*x*(Bi_2Se_3)=0÷0.78	1052-123*x+ 100*x^2-140*x^3	8
	Bi_2S_3-Bi_2Se_3, liquidus Bi_2Se_3, x=*x*(Bi_2Se_3)=0.78÷1	590+720*x-331*x^2	9

analytical option of the OriginLab computer program. The temperature dependences of the

crystallization surface are determined as a function

$$T=f(x, y) \quad (1)$$

where: x -is the relative mole fraction BiI_3: $y=x(Bi_2Se_3/[x(Bi_2S_3)+x(Bi_2Se_3)]$.

The obtained analytical expressions for the ternary system, the BiI_3-Bi_2S_3-Bi_2Se_3 and its binary boundary systems are given in Tables 1 and 2. Modeling is carried out in this order. First, the temperature dependences on the composition are determined for the liquids of binary boundary systems. Next, on the basis of using the experimental ternary, the BiI_3-Bi_2S_3-Bi_2Se_3 system defined function T=f (x, y).

Table 2. Analytical dependencies for liquidus surfaces of the BiI_3-Bi_2S_3-Bi_2Se_3 system

Compound liquidus surface	T,K=f(x,y); x=x(BI_3); y= x(Bi_2Se_3/[x(Bi_2S_3)+ x(Bi_2Se_3)]	Eq.N.
likvidus α(Bi_2S_3)	(1052-123*y+100*y^2-140*y^3)*(1-x)^0.306 x=0-0.2, y=0-0.78	10
likvidus β(Bi_2Se_3)	(979-173*x-182*x^2)*y^0.12 x=0-0.584, y=0.78-1	11
δ($Bi_{19}S_{27}J_3$)	(993+106*x-600*x^2)*(1-y)*0.038 x=0.2-0.65, y=0-0.8	12
liquidus γ($BiS_{1-x}Se_xJ$)	(1830-4334*x+6317*x^2-3192*x^3)*y+(574+920*x-860*x^2)*(1-y)+98*x*(1-x)*y*(1-y) S side 0.65-0.95, Se side 0.584-0.95, y=0-1	13
liquidus BiI_3,	(503+178*x)*y+(248+433*x)*(1-y) x=0.955÷1	14

Binary boundary systems

The boundary quasi-binary constituents of the system BiI_3-Bi_2S_3-Bi_2Se_3 have been studied in detail [37, 44, 45]. In the system Bi_2S_3–BiI_3 (Fig.1), two ternary compounds, BiSI and $Bi_{19}S_{27}I_3$, form, which melt with decomposition by peritectic reactions at 808 and 990 K, respectively [37]. The compound BiSI crystallizes in the orthorhombic symmetry, and $Bi_{19}S_{27}I_3$ has a hexagonal lattice. In the system Bi_2Se_3–BiI_3 (Fig.2), one compound BiSeI, is formed, which melts incongruently at 818 K [44]. Quasi-binary system of Bi_2S_3-Bi_2Se_3 (Fig.3) eutectic type with a wide solubility region in the solid state [45]. The phase diagrams of the quasi-binary boundary systems BiI_3-Bi_2S_3, BiI_3-Bi_2Se_3 and Bi_2S_3-Bi_2Se_3 and their analytical dependences for liquidus lines are shown in Table 1.

3.1.2. 3D modeling of the liquidus surface

The analytical dependences for 3D modeling of the liquidus surfaces of the BiI_3, Bi_2S_3, Bi_2Se_3, BiSI, $Bi_{19}S_{27}I_3$, and BiSeI phases are given in Table 2 (equations 10-14). These equations allow visualizing the crystallization surfaces of all phases (Fig. 4).

As can be seen from Fig. 4, the liquidus surface of the system consists of five primary crystallization fields. Four of the largest fields correspond to the primary crystallization of the α-, β-, γ-, and δ-phases from the melt. Meanwhile, the liquidus surface of the BiI_3 compound is nearly degenerate near the corresponding vertex in the compositional triangle.

In contrast to the binary compounds in the system, all three ternary compounds undergo incongruent melting via peritectic reactions. Consequently, the primary crystallization fields of the γ- and δ-phases (fields 3 and 4) are located outside their respective compositional (homogeneity) ranges. The constructed phase diagram thus enables the selection of appropriate liquid-phase compositions for crystal growth.

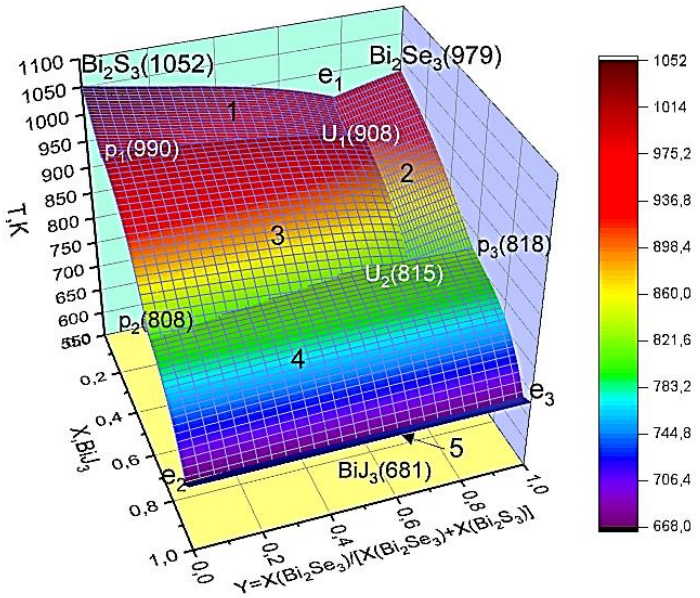

Fig. 4. 3D model of crystallization surfaces of the Bi_2S_3-Bi_2Se_3-BiI_3 system, visualized by equations 10-14 in Table 2.

1. Liquidus surface of solid solutions based on α-(Bi_2S_3)
2. Liquidus surface of solid solutions based on β-(Bi_2Se_3)
3. Liquidus surface of solid solutions based on δ-($Bi_{19}S_{27}J_3$)
4. Liquidus surface of solid solutions based on γ-($BiS_{1-x}Se_xI$)
5. Liquidus surface of BiI_3

The liquidus surfaces of the various phases are delineated by a set of monovariant equilibrium curves and invariant equilibrium points. Detailed information on the nature and temperatures of all identified invariant and monovariant equilibria is collected in Table 3.

Table 3. Non- and monovariant equilibria in the Bi_2S_3-BiI_3-Bi_2Se_3 ternary system

Curve and point in Fig. 4	Equilibrium	T,K
P_1	$L + Bi_2S_3 \leftrightarrow Bi_{19}S_{27}I_3$	990
P_2	$L + Bi_{19}S_{27}I_3 \leftrightarrow BiSI$	808
P_3	$L + Bi_2Se_3 \leftrightarrow BiSeI$	818
e_1	$L \leftrightarrow \alpha + \beta$	950
e_2	$L \leftrightarrow BiSI + BiI_3$	670
e_3	$L \leftrightarrow BiSeI + BiI_3$	665
U_1	$L + \alpha \leftrightarrow \beta + \delta$	908
U_2	$L + \beta \leftrightarrow \gamma + \delta$	815
P_1U_1	$L + \alpha \leftrightarrow \delta$	990-908
e_1U_1	$L \leftrightarrow \alpha + \beta$	950-908
U_1U_2	$L \leftrightarrow \beta + \delta$	908-815
P_3U_2	$L + \beta \leftrightarrow \gamma$	818-815
U_2P_2	$L + \delta \leftrightarrow \gamma$	815-808
e_2e_3	$L \leftrightarrow \gamma + BiI_3$	670-665

3. 2. Isopleth Sections

Based on the projection of the liquidus surface (Fig. 4) and the phase diagram of solid-phase equilibria of the system, it is possible to construct any isopleth or isothermal section of the volumetric T–x–y diagram.

Figures 5–7 present, as examples, modeled T–x diagrams of the isopleth sections

for the Bi_2S_2Se-BiI_3, Bi_2SSe_2-BiI_3, and $Bi_2S_{0,5}Se_{0,5}$-BiI_3 systems. For each section, DTA results obtained from several thermally treated samples are indicated (points). As can be seen, the limited number of experimental DTA data points is in good agreement with the modeled T–x diagrams.

Let us analyze the presented isopleth sections in the context of the 3D model of the liquidus surface and the solid-phase equilibria diagram. As shown in Fig. 5, along the Bi_2S_2Se-BiI_3 section, moving from left to right, primary crystallization from the melt proceeds as follows: the α-phase based on Bi_2S_3 (0–20 mol% BiI_3), the δ-phase based on $Bi_{19}S_{27}I_3$ (20–60 mol% BiI_3), γ-phase solid solutions of $BiS_{1-x}Se_xI$ (60–98 mol% BiI_3), and finally the BiI_3 compound. Below the liquidus curves, crystallization continues via the monovariant peritectic reactions L+α↔δ (Fig. 4, curve e_1U_1), L+β↔γ (curve P_2U_2), and the monovariant eutectic reaction L↔γ+BiI_3 (curve e_2e_3). As a result of these reactions, three-phase regions L+α+δ, L+δ+γ, and L+γ+BiI_3 are formed on the phase diagram (Fig. 5). Crystallization is completed by the formation of single-phase δ and γ alloys at compositions of 10 and 50 mol% BiI_3, respectively, while in intermediate composition ranges, two-phase alloys α+δ, γ+δ, and γ+BiI_3 are formed. The crystallization processes along the Bi_2SSe_2–BiI_3 section (Fig. 6) are qualitatively similar to those described above.

For the $Bi_2S_{0.5}Se_{0.5}$-BiI_3 section (Fig. 7), the liquidus consists of three curves corresponding, from left to right, to the primary crystallization of the β-phase based on Bi_2Se_3 (0–55 mol% BiI_3), the γ-phase (55–98 mol% BiI_3), and the BiI_3 compound. Following the primary crystallization of the β-phase, the process continues via the monovariant eutectic reactions L↔α+β (curve e_1U_1) and L↔β+γ (curve U_1U_2), and is completed through the nonvariant transition reactions L+α↔β+δ (U_1, 908 K) and L+δ↔β+γ (U_2, 815 K). Under conditions of liquid-phase deficiency, these reactions terminate in the subsolidus region, leading to the formation of three-phase fields α+β+δ and β+γ+δ.

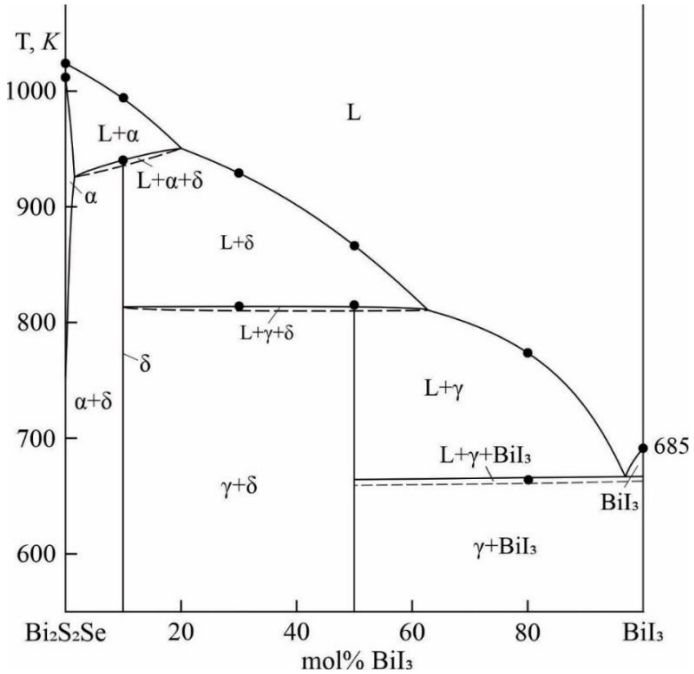

Fig. 5. Bi_2S_2Se-BiI_3 isopleth section

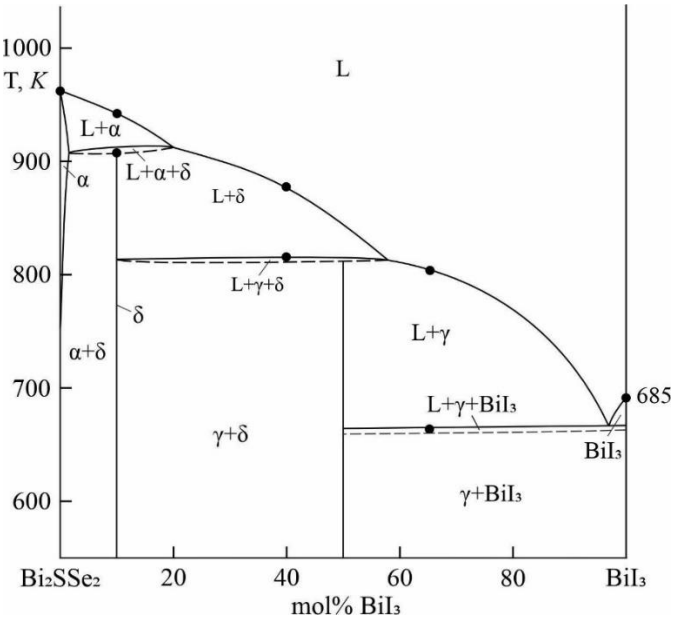

Fig. 6. Bi_2SSe_2–BiI_3 isopleth section

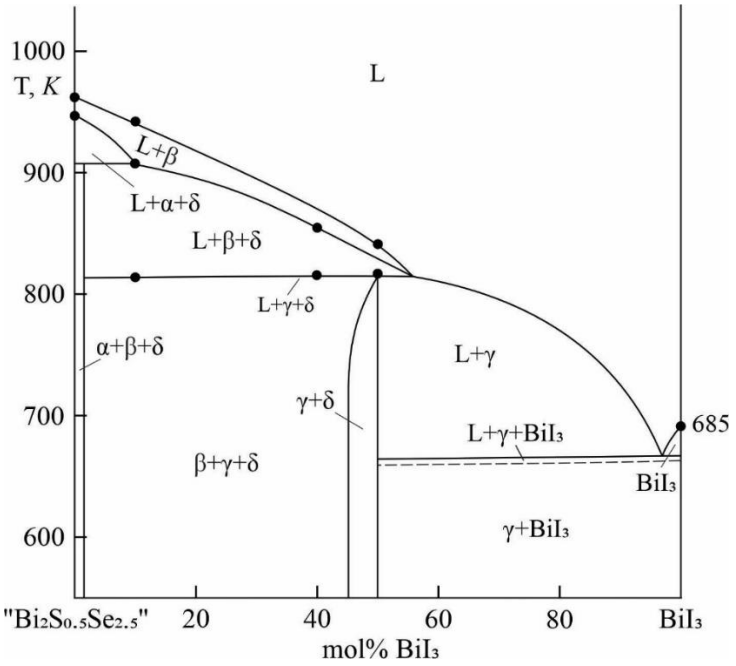

Fig. 7. $Bi_2S_{0.5}Se_{0.5}$-BiI_3 isopleth section

Conclusion

In this work, analytical modeling and 3D visualization of the liquidus surface of the Bi_2S_3-Bi_2Se_3-BiI_3 (A) system were performed using phase diagrams of boundary quasi-binary systems and differential thermal analysis (DTA) data for selected alloys along several internal sections. The primary crystallization fields of the phases, as well as the types and coordinates of non- and monovariant equilibria, were determined, and several polythermal sections of the T-x-y phase diagram were constructed. The obtained analytical dependencies for the liquidus curves of the phases in the boundary

systems, derived from the solid-phase equilibrium diagram of system (A), as well as for the liquidus surfaces of solid solutions and intermediate phases $BiS_{1-x}Se_xI$ and $Bi_{19}S_{27(1-x)}Se_{27x}I_3$ based on Bi_2S_3 and Bi_2Se_3 compounds in system (A), enabled 3D visualization of all elements of the phase diagram within a single graph. The analytical dependencies were obtained using the 2D and 3D capabilities of the OriginLab program. The tabular data, presented in the form of matrices of dimensions 100×100=10.000 and 50×50=2.500, can be used to select the optimal composition and temperature parameters for the synthesis of binary and ternary phases in the (A) system.

References

1. Ganose A.M., Butler K.T., Walsh A. et al. Relativistic electronic structure and band alignment of BiSI and BiSeI: candidate photovoltaic materials. *J. Mater. Chem.* A. 2016. V. 4. P. 2060-2068. https://doi.org/10.1039/C5TA09612J
2. Audzijonis A., Zaltauskas R., Sereika R. et al. Electronic structure and optical properties of BiSI crystal. *J. Phys. Chem. Solids*. 2010. V. 71. P. 884-891. https://doi.org/10.1016/j.jpcs.2010.03.042
3. Audzijonis A., Gaigalas G., Zigas L. et al. Electronic structure and optical properties of BiSeI crystal. *Phys. Status Solid Basics.* 2009. V. 246. №7. P. 1702-1708. https://doi.org/10.1016/j.jpcs.2010.03.042
4. Mistewicz K., Das T.K., Nowacki B. et al. Bismuth sulfoiodide (BiSI) nanorods: synthesis, characterization, and photodetector application. *Sci. Rep.* 2023. V. 13. P. 8800. https://doi.org/10.1038/s41598-023-35899-7
5. Kunioku H., Higashi M., Abe R. Low Temperature Synthesis of Bismuth Chalcohalides: Candidate Photovoltaic Materials with Easily, Continuously Controllable Band gap. *Sci. Rep.* 2016. V. 6. P. 32664. https://doi.org/10.1038/srep32664
6. Khan W., Hussain S., Minar J. et al. Electronic and Thermoelectric Properties of Ternary Chalcohalide Semiconductors: First Principles Study. *J. Electron. Mater.* 2018. V. 47. P. 1131–1139. https://doi.org/10.1007/s11664-017-5884-z
7. Koc H., Palaz S., Mamedov A. M. et al. Optical, electronic, and elastic properties of some $A^5B^6C^7$ ferroelectrics (A=Sb, Bi; B=S, Se; C=I, Br, Cl): First principle calculation. *Ferroelectrics.* 2017. V. 511. P. 22-34. https://doi.org/10.1080/00150193.2017.1332967
8. Peng B., Xu K., Zhang H. et al. 1D SbSeI, SbSI, and SbSBr with High Stability and Novel Properties for Microelectronic, Optoelectronic, and Thermoelectric Applications. *Adv. Theory Simul.* 2018. V. 1. №1. P. 1700005. https://doi.org/10.1002/adts.201700005
9. Ishizaka K., Bahramy M.S., Murakawa H. et al. Giant Rashba-type spin splitting in bulk BiTeI. *Nat. Mater.* 2011. V. 10. №7. P. 521-526. https://doi.org/10.1038/nmat3051
10. Landolt G., Eremeev S.V., Koroteev Y.M. et al. Disentanglement of Surface and Bulk Rashba Spin Splittings in Noncentrosymmetric BiTeI. *Phys. Rev. Lett.* 2012. V. 109. P. 116403.https://doi.org/10.1103/PhysRevLett.109.116403
11. Wu L., Yang J., Zhang T. et al. Enhanced thermoelectric performance in the Rashba semiconductor BiTeI through band gap engineering. *J. Phys.: Condens. Matter.* 2016. V. 28. №8. P. 085801.https://doi.org/ 10.1088/0953-8984/28/8/085801
12. Hajra D., Sailus R., Blei M. et al. Epitaxial Synthesis of Highly Oriented 2D Janus Rashba Semiconductor BiTeCl and BiTeBr Layers. *ACS Nano.* 2020. V. 14. №11. P. 15626-15632. https://doi.org/10.1021/acsnano.0c06434
13. Qu J., Cuddy E. F., Han X. et al. Screening of Polar Electron-Phonon Interactions near the Surface of the Rashba Semiconductor BiTeCl. *Phys. Rev. Lett. V.* 2024. V. 133. P. 106401. https://doi.org/10.1103/PhysRevLett.133.106401
14. Babanly M.B., Yusibov Y.A., Imamaliyeva S.Z. et al. Phase Diagrams in the Development of the Argyrodite Family Compounds and Solid Solutions Based on Them. *J. Ph. Equilibria Diffus.* 2024. V. 45. P. 228–255. https://doi.org/10.1007/s11669-024-01088-w
15. Babanly M.B., Mashadieva L.F., Imamaliyeva S.Z. et al. Complex copper-based chalcogenides: a review of phase equilibria and thermodynamic properties. *Condens. Matter and Interphases.* 2024. V. 26. №4. P. 579-619. https://doi.org/10.17308/kcmf.2024.26/12367
16. Babanly M.B., Mashadiyeva L.F., Imamaliyeva S.Z. et al. Thermodynamic properties of complex copper chalcogenides. *Chem. Probl.* 2024. V. 3. P. 243-280. https://doi.org/10.32737/2221-8688-2024-3-243-280
17. Babanly M.B., Mashadiyeva L.F., Babanly D.M. et al. Some Issues of Complex Studies of Phase Equilibria and Thermodynamic Properties in Ternary Chalcogenide Systems Involving Emf Measurements (Review). *Russ. J. Inorg. Chem.* 2019. V. 64. №13. P. 1649-1671. https://doi.org/10.1134/S0036023619130035
18. Babanly M.B., Chulkov E.V., Aliev Z.S. et al. Phase diagrams in materials science of topological insulators based on metal chalcogenides. *Russ. J. Inorg. Chem.* 2017. V. 62. P. 1703-1729.

https://doi.org/10.1134/S0036023617130034
19. Ahmadov E.J. Physico-chemical interaction in the BiSI–BiTeI system. *Az. Chem. J*. 2020. V. 1. P. 36-40. https://doi.org/doi.org/10.32737/0005-2531-2020-1-36-40
20. Ahmadov E.J., Babanly D.M., Aliyev Z.S. et al.Phase equilibria in the system SbTeI-BiTeI. New. Mat. Compd. Appl. 2019. V. 3. P. 87-93.
21. Safarov F., Babanly D., Robert J. et al. Phase equilibria in $MnSb_2Te_4$-$GeSb_2Te_4$ system and magnetic properties of $Mn_{1-x}GexSb_2Te_4$ solid solutions. *J. Magn. Magn. Mater*. 2026. V. 645. P. 173969. https://doi.org/10.1016/j.jmmm.2026.173969
22. Orujlu E.N., Babanly D.M., Ahmadov E.J. et al. SnTe-Bi_2Te_3-Te system: Phase equilibria and thermodynamic properties of SnTe-rich ternary phases. *J. Alloys Compd.* 2026. V. 1050. P. 185754. https://doi.org/10.1016/j.jallcom.2025.185754
23. Babanly D.M., Mammadli P.R., Dashdiyeva G.B. et al. Phase equilibria in the $CuSbS_2$-Sb_2S_3-SbSI composition range of the Cu-Sb-S-I quaternary system. *New. Mat. Compd. Appl*. 2025. V. 9. №1. P. 40-49. https://doi.org/10.62476/nmca.9140
24. Aliev Z.S., Ahmadov E.C., Babanly D.M. et al. The Bi_2Se_3-Bi_2Te_3-BiI_3 system: synthesis and characterization of the $BiTe_{1-x}Se_xI$ solid solutions. *Calphad.* 2019. V. 66. P. 101650. https://doi.org/10.1016/j.calphad.2019.101650
25. Ahmadov E.J., Aliev Z.S., Babanly D.M. et al.The Quasi-Ternary system Bi_2S_3–Bi_2Te_3–BiI_3. *Russ. J. Inorg. Chem.* 2021. V. 66. P. 538-549.https://doi.org/10.1134/S0036023621040021
26. Ahmadov E.J., Orujlu E.N., Babanly D.M. et al. Phase equilibria of the $Sb_2Te_3+2BiI_3 \leftrightarrow Bi_2Te_3+2SbI_3$ reciprocal system: Synthesis and characterization of the cation-substituted $Bi_{1-x}Sb_xTeI$ solid solutions. *J. Alloys Compd.* 2022. V. 929. P. 167388. https://doi.org/10.1016/j.jallcom.2022.167388
27. Mammadov F.M., Babanly D.M., Imamaliyeva S.Z. et al. Solid-phase equilibria in the FeS-In_2S_3-S system, thermodynamic properties of the $FeIn_2S_4$ compound and $(FeS)_{1-x}(In_2S_3)_x$ solid solutions. *J. Chem. Thermodyn*. 2026. V. 213. P. 107585. https://doi.org/10.1016/j.jct.2025.107585
28. Mammadov F.M., Babanly D.M., Imamaliyeva S.Z. et al. Solid-phase relations in the FeSe-Ga_2Se_3-Se system and thermodynamic investigation of the $FeGa_2Se_4$ compound and $(FeSe)_{1-x}(Ga_2Se_3)_x$ solid solutions. *Chem. Thermodyn. Therm. Anal*. 2025. V. 19. P. 100207.https://doi.org/10.1016/j.ctta.2025.100207
29. Qurbanov A., Ahmadov E., Alverdiyev I. et al. Phsico-chemical interaction in the BiSI-BiSeI system. *BSU-CMS.* 2024. V. 1. №4. P. 6-12. https://doi.org/10.30546/209501.201.2024.1.04.061
30. Qurbanov A.A., Ahmadov E.J., Aghazade A.I. et al. Phase equilibria in the $Bi_{19}S_{27}I_3$-"$Bi_{19}Se_{27}I_3$" system and characterization of solid solutions. *Az. Chem. J.* 2026. V. 2. P. 145-152. https://doi.org/10.32737/0005-2531-2026-2-145-152
31. Qurbanov A.A., Ahmadov E.J., Shukurova G.M. et al. Thermodynamic study of the BiSI-BiSeI system by the electromotive force method. *Condensed Matter and Interphases.* 2026. V. 28. №1. P. 46-56. https://doi.org/10.17308/kcmf.2026.28/13590
32. Qurbanov A.A., Ahmadov E.J., Mammadova S.R. et al. Solid-phase equilibria in the Bi_2S_3-Bi_2Se_3-BiI_3 system and thermodynamic properties of solid solutions based on $Bi_{19}S_{27}I_3$. *New. Mat. Compd. Appl.* 2026. V. 10. №1. P. 209-222.https://doi.org/10.62476/nmca.101209
33. Leenson I.A. Sublimination of Iodine at Various Pressures: Mutlipurpose Experiments in Inorganic and Physical Chemistry. *J. Chem. Educ.* 2005. V. 82. P. 241. https://doi.org/10.1021/ed082p241
34. Meyer B. Elemental sulfur. *Chem. Rev.* 1976. V. 76. P. 367-388. https://doi.org/10.1021/cr60301a003
35. Fujisaki H., Westmore J.B., Tickner A.W. Mass spectrometric study of subliming selenium, *Can. J. Chem.* 1966. V. 44. P. 3063-3071. https://doi.org/10.1139/v66-448
36. Massalski T.B., Okamoto H., Subramanian P.R. et al. Binary Alloy Phase Diagrams. 2nd ed., ASM International, Materials Park. OH. USA. 1990.
37. Aliev Z.S., Musayeva S.S., Jafarli F.Y. et al. The phase equilibria in the Bi–S–I ternary system and thermodynamic properties of the BiSI and $Bi_{19}S_{27}I_3$ ternary compounds. *J. Alloys Compd.* 2014. V. 610. P. 522-528. https://doi.org/10.1016/j.jallcom.2014.05.015
38. Valitova N.R., Aleshin V.A., Popovkin B.A., Novoselova A.V. p–T–x Phase Diagram of the System Bismuth Iodide-Bismuth Telluride. Izv. Akad. Nauk SSSR. Neorg. Mater. 1976. V. 12. P. 225-228.
39. Mammadov A.N., Sharifova U.N., Babanly M.B. et al. Application of fuzzy logic theory to thermodynamic modeling of phase equilibrium and oxidation-reduction reactions. *Az. Chem. J.* 2025. №2. P. 36-51. https://doi.org/10.32737/0005-2531-2025-2-36-51
40. Aslanli S.R., Babanly K.N., Ashirov G.M. et al. Ag_2Se-$SiSe_2$-$SnSe_2$ System: Experimental Study and 3D Visualization of the Phase Diagram. *Russ. J. Inorg. Chem*. 2025. V. 70. №12. P. 2023-2033. https://doi.org/ 10.1134/S0036023625602156

41. Aghazade A.I., Babanly V.I., Gojayeva I.M. et al. 3D modeling of phase diagram of the ternary SnTe-PbTe-Bi_2Te_3 system. *Azerb. Chem. J.* 2023. №2. P. 62–68. https://doi.org/10.32737/0005-2531-2023-2-62-68
42. Aghazade A.I., Rustamova S.M., Gojayeva I.M. et al. Multi-3D modeling of phase diagram of PbTe-Bi_2Te_3-Sb_2Te_3 system. *Chem. Probl.* 2023. V. 21. №4. P. 353–360. https://doi.org/ 10.32737/2221-8688-2023-4-353-360
43. Ahmadov E.J., Mammadov A.N., Guliyeva S.A., Babanly M.B. Modeling of phase diagram of the system BiI_3-Bi_2S_3-Bi_2Te_3. New. Mat. Compd. Appl. 2021. V. 5. №1. P. 5–11.
44. Petasch U., Goebel H., Oppermann H. Untersuchungen zum quasibinären System Bi_2Se_3/BiI_3. *Z. Anorg. Allg. Chem*. 1998. V. 624. P. 1767.
45. Benher Z.R., Gardonio S., Fanetti M. et al. Electronic properties of phases in the quasi-binary Bi_2Se_3–Bi_2S_3 system. J. Mater. Chem. C. 2021. V. 9. P. 3058. https://doi.org/10.1039/D0TC05121G

Bi_2S_3-Bi_2Se_3-BiI_3 SİSTEMİNİN T-x-y FAZA DİAQRAMININ ANALİTİK MODELLƏŞDİRİLMƏSİ VƏ 3D VİZUALLAŞDIRILMASI

A.A.Qurbanov, E.C.Əhmədov, A.İ.Ağazadə, G.F.Həsənov, F.S.İbrahimova, İ.C.Alverdiyev, A.N.Məmmədov

Sərhəd kvazibinar sistemlərin faza diaqramları Bi_2S_3–Bi_2Se_3–BiI_3 (A) qatılıq üçbucağı daxilində seçmə tərkiblər üçün məhdud sayda DTA məlumatları və (A) sisteminin bərkfaza tarazlıqları diaqramı əsasında sərhəd sistemlərdə fazaların likvidus əyriləri üçün, həmçinin (A) sistemində Bi_2S_3, Bi_2Se_3 birləşmələri əsasında bərk məhlulların və $BiS_{1-x}Se_xI$ və $Bi_{19}S_{27(1-x)}Se_{27x}I_3$ aralıq fazalarının likvidus səthləri üçün analitik tənliklər alınmışdır. Alınmış tənliklər əsasında (A) sisteminin likvidus səthinin 3D vizuallaşması həyata keçirilmiş, sistemdə mövcud olan non- və monovariant tarazlıqların tipləri və koordinatları müəyyən edilmişdir. Likvidus səthinin 3D modeli əsasında T-x-y faza diaqramının bəzi politermik kəsikləri qurulmuş və məhdud sayda nümunlərin DTA nəticələri ilə təsdiq edilmişdir. Təqdim edilən nəticələr tənzimlənən tərkib və xassələrə malik $BiS_{1-x}S_xI$ və $Bi_{19}S_{27(1-x)}Se_{27x}I_3$ bərk məhlullarının sintezi və krsitallarının yetişdirilməsində istifadə oluna bilər.

Açar sözlər: *bismutun tio- və selenoyodidləri, faza diaqramı, likvidus səthi, 3D analitik modelləşdirmə, bərk məhlullar*.